Improving spatial resolution in fiber Raman distributed temperature sensor by using deconvolution algorithm

Lei Zhang (张 磊)*, Xue Feng (冯 雪), Wei Zhang (张 巍), and Xiaoming Liu (刘小明)

State Key Laboratory on Integrated Optoelectronics/Tsinghua National Laboratory for Information Science and Technology, Tsinghua University, Beijing 100084, China

**E-mail: l-z04@mails.thu.edu.cn*

Received November 17, 2008

The deconvolution algorithm is adopted on the fiber Raman distributed temperature sensor (FRDTS) to improve the spatial resolution without reducing the pulse width of the light source. Numerical simulation shows that the spatial resolution is enhanced by four times using the frequency-domain deconvolution algorithm with high temperature accuracy. In experiment, a spatial resolution of 15 m is realized using a master oscillator power amplifier light source with 300-ns pulse width. In addition, the dispersion-induced limitation of the minimum spatial resolution achieved by deconvolution algorithm is analyzed. The results indicate that the deconvolution algorithm is a beneficial complement for the FRDTS to realize accurate locating and temperature monitoring for sharp temperature variations.

OCIS codes: 060.2370, 100.1830.
doi: 10.3788/COL20090707.0560.

Distributed fiber optic sensor has been intensively studied during the past years[1−3] due to its wide range of applications such as leakage detection of oil pipelines, monitoring of high voltage power cables, and health monitoring of dam. Based on the spontaneous Raman scattering in optical fibers and the technique of optical time domain reflectometry (OTDR)[4], fiber Raman distributed temperature sensor (FRDTS) can measure the temperature distribution over a long distance of tens of kilometers continuously with a high spatial resolution of several meters.

Spatial resolution is an important parameter to evaluate the performance of FRDTS. It has been analyzed that the received anti-Stokes Raman backscattered signal intensity can be expressed as a convolution of the input pulse profile and the temperature distribution along the fiber if the bandwidth of optoelectronic receiving system and the followed electronic system is high enough[5]. In conventional FRDTS, however, the anti-Stokes backscattered signal intensity[6] is treated as the product of input light power and the temperature distribution. This approximation is valid only when the light pulse length is much shorter than the spatial temperature variation length along the fiber. Therefore, the spatial resolution of conventional FRDTS is limited by the light pulse width with enough signal receiving bandwidth. The improvement of spatial resolution can only be achieved by reducing the light pulse width. Then if both input pulse peak intensity and measurement time keep constant, the backscattered light intensity and the signal-to-noise ratio (SNR) will be decreased unavoidably, which would deteriorate the temperature resolution[7]. So it would be very valuable to improve the performance of FRDTS if the spatial resolution could be improved without decreasing the pulse width. The deconvolution algorithm has been adopted to achieve similar aim in Brillouin distributed fiber-optic temperature sensing system[8] and polarization optical time domain reflectometer system[9]. And it has been validated that the temperature or strain variation in small regions can be identified exactly in the OTDR system.

In this letter, the frequency-domain deconvolution algorithm so-called ASFDA, which is proposed by Bennia *et al.*[10], is adopted to improve the spatial resolution of the FRDTS without reducing the pulse width. Unlike that in Ref. [10], different filter parameters are chosen for different frequency intervals according to the proportion of signal components in frequency domain. In addition, the convolutional expression is also deduced for bi-channel measurement which is widely used in FRDTS. Then based on ASFDA, the spatial resolution improvement is demonstrated numerically and experimentally by comparing it with that of conventional FRDTS. Finally, the minimum spatial resolution achieved by using deconvolution algorithm for different sensing distances is discussed through the analysis of dispersion in sensing fiber.

According to Ref. [5], if the bandwidth of the signal receiving system is high enough, the expression of the measured anti-Stokes Raman backscattered light power $P_{\mathrm{a-s}}(T,t)$ can be written as a convolution of input pulse and the temperature distribution by taking the waveform of input optical pulse into account:

$$P_{\mathrm{a-s}}(T,t) = P_0(t) \otimes g_{\mathrm{a-s}}(T,t), \quad (1)$$

$$g_{\mathrm{a-s}}(T,t) = \frac{v}{2} S K_{\mathrm{a-s}} R_{\mathrm{a-s}}(T,t) \exp\left[-\frac{v}{2}(\alpha_0 + \alpha_{\mathrm{a-s}})t \right], \quad (2)$$

where $P_0(t)$ is the power profile of the input light pulse; $g_{\mathrm{a-s}}(T,t)$ represents the function of fiber temperature distribution including Raman backscattering and light propagation; v is the light velocity in the fiber; $K_{\mathrm{a-s}}$ and S are the coefficient and capture fraction of the anti-Stokes Raman backscattering, respectively; α_0 and $\alpha_{\mathrm{a-s}}$ are fiber attenuation coefficients at wavelengths of the launched pulses and the anti-Stokes scattering, respectively; $R_{\mathrm{a-s}}(T,t)$ is the Bose-Einstein factor, which is a known function of temperature T and propagation time t[11]. The temperature distribution along the fiber can be calculated by the relation between distance d and propagation time $t = 2d/v$[12]. So the actual function of fiber

temperature distribution can be obtained from $g_{\mathrm{a-s}}(T,t)$ by using deconvolution algorithm.

ASFDA is a kind of deconvolution methods, by which the estimation of $g_{\mathrm{a-s}}(T,t)$ can be achieved in the case of the received signal mixing electrical noise. By using ASFDA, the solution of Eq. (1) can be written as

$$H(\omega)=\frac{Y(\omega)}{X(\omega)}\cdot\frac{1}{1+\lambda/|X(\omega)|^2},\tag{3}$$

where $X(\omega)$, $H(\omega)$, and $Y(\omega)$ are the Fourier transforms of $P_0(t)$, $g_{\mathrm{a-s}}(T,t)$, and $P_{\mathrm{a-s}}(T,t)$, respectively, and the filter parameter λ is a positive constant. Generally, the temperature variation always lies in the low frequency regions compared with the noise. With the frequency increasing, the ratio of power spectrum between noise and $g_{\mathrm{a-s}}(T,t)$ is increased. So different from Ref. [10], two values of filter parameter λ are selected for different frequency intervals to optimize the results of deconvolution. A small value of λ is chosen in the low frequency region while a large value in the high frequency band. The boundary of the frequency intervals can be decided in advance according to the spatial resolution of FRDTS to be achieved. The values of λ should be carefully chosen before temperature measurement according to the obtainable SNR of different FRDTSs.

In an actual FRDTS system, the backscattered light power fluctuation due to undesired effects is unavoidable, such as attenuation coefficient variation along the fibers, lumped loss, reflection of fiber splicing points, and so on. Hence, bi-channel measurement technique is widely used[5], in which the backward Rayleigh scattering light is used as the reference signal to compensate the undesired backscattered light power fluctuation. The convolutional expression is also deduced for bi-channel measurement. The result of bi-channel measurement can finally be expressed as

$$\frac{P_{\mathrm{a-s}}(T,t)/P_{\mathrm{R}}(T,t)}{P_{\mathrm{a-s}}(T_0,t)/P_{\mathrm{R}}(T_0,t)}\int_0^{\tau_0}P_0(\tau)R_{\mathrm{a-s}}(T_0,t-\tau)\mathrm{d}\tau=\int_0^{\tau_0}P_0(\tau)R_{\mathrm{a-s}}(T,t-\tau)\mathrm{d}\tau,\tag{4}$$

where the subscription R represents Rayleigh backscattered light, and T_0 is a certain temperature acting as calibration in the temperature sensing process[5]. It can be seen that all the items on the left hand side of Eq. (4) are known or measurable, and the right hand side is exactly a convolution operation. So based on the measured data and Eq. (4), the temperature information can be restored by using deconvolution algorithm.

The performance of the adopted method is simulated using ASFDA and compared with the conventional method[5,6]. The length of sensing fiber is 1 km in simulation. The attenuation coefficients of the launched light and anti-Stokes light are 0.25 and 0.4 dB/km, respectively. The main part of the fiber is under a temperature of 298 K, except three sections under an abnormal temperature of 318 K, whose lengths are 1.5, 2, and 3 m, respectively. The probe optical pulse is set as five-order super-Gaussian shape, and the full-width at half-maximum (FWHM) of the pulse is 60 ns, corresponding to a conventional spatial resolution of 6 m. The sampling interval is 0.05 m. The Gaussian white noise is added on the received signal to simulate the noise in optical detection and electrical processing.

Figure. 1(a) shows the measured temperature distribution by conventional method. It can be seen that in the region with uniform temperature, the mean measured temperature agrees well with the simulation result, with a standard deviation of 0.35 K due to the Gaussian noise. The measured abnormal temperature values are 303, 305, and 308 K, respectively. Since the sections of abnormal temperature are shorter than the probe pulse, the measured sections of temperature variation are much wider than the real lengths and the measured temperatures are the mean values in the range of 6 m. The divergency of the measured temperatures and section lengths reflects the intrinsic problem of conventional method.

Figure 1(b) shows the results using ASFDA with the Rayleigh backscattered light as a reference. The boundary of the frequency intervals is set at 50 MHz. The values of λ are 1 ($<$50 MHz) and 10^8 ($\geq$50 MHz), respectively. It can be seen that the temperature variation in a section as shorter as 1.5 m can be restored accurately by the ASFDA. The restored temperatures of the three abnormal sections are 317.5, 318.4, and 317.6 K, respectively, showing a good agreement with the simulation results. It demonstrates that a spatial resolution as high as 1.5 m can be achieved by ASFDA using a pulse width of 60 ns, which is a quarter of the spatial resolution of the conventional method. On the other hand, it can be seen that the noise of the temperature curve is a little higher than the one in Fig. 1(a).

In order to examine the restored temperature accuracy achieved by ASFDA, the statistical data of the difference between the actual temperature and the restored one are calculated according to the simulation results of 100 times, as shown in Fig. 2. In simulation, the temperature is varied from 303 to 348 K in a fiber section of 1.5 m. It can be seen that the mean values of the restored temperature are always a little less than the actual ones. The temperature accuracy is better than 0.3 K. The error bars in Fig. 2 represent the temperature standard deviation at different abnormal temperature levels, which is about 0.65 K. The standard deviation is higher than that using conventional method, because some unwanted noise is retrieved by the deconvolution algorithm besides the fast variation of temperature signal.

Compared with the results using conventional method,

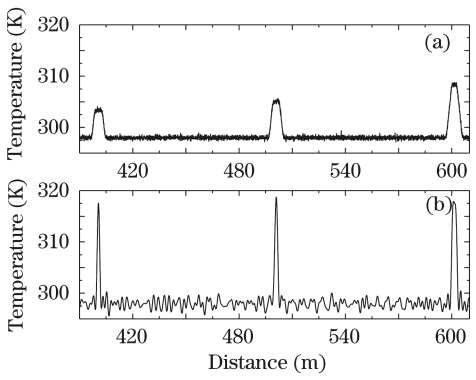

Fig. 1. Simulation results restored by (a) conventional method and (b) ASFDA.

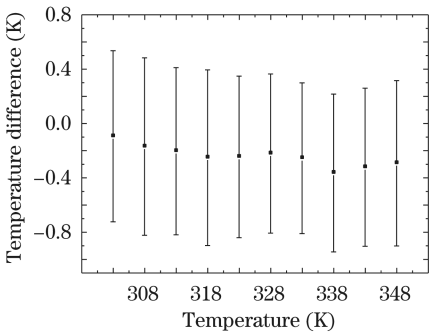

Fig. 2. Restored temperature difference by ASFDA under different temperatures.

the simulation results demonstrate that the data processing method based on ASFDA can improve the spatial resolution and the restored temperature accuracy obviously, with a little cost on the noise of the restored temperature curves (the temperature standard deviation rises from 0.35 to 0.65 K). Hence, the adopted method provides a valuable way to realize accurate locating and temperature monitoring for the sharp temperature variations.

Experiments were performed using the arrangement shown in Fig. 3. The 1.55-μm master oscillator power amplifier (MOPA) light source with a peak power of 7 W was used. The pulse width was 300 ns, corresponding to the spatial resolution of 30 m using conventional method. In order to prevent coherent effects, a Fabry-Perot laser diode with 3-nm FWHM linewidth was used as the master oscillator. The probe light pulses were coupled into the sensing fiber through an optical circulator. The anti-Stokes Raman backscattered signal at 1.45 μm and Rayleigh backscattered signal at 1.55 μm were extracted by the wide spectral band-pass filter (BPF) with FWHM linewidth of 20 nm and then detected by the sensitive InGaAs PIN detectors in conjunction with transimpedance amplifiers with the electrical bandwidth of about 100 MHz. The sampling rate of analog-to-digital converter (ADC) was 50 MS/s.

A 300-m-long single-mode fiber (SMF) was used as the sensing fiber. A 15-m-long section of the fiber was placed in an oven and the temperature was changed from 311 to 331 K in 5-K steps. The rest of the fiber was maintained at room temperature of about 298 K. After the average of 8×10^5 single-pulse traces, the temperature distribution obtained from conventional method is shown in Fig. 4. From the result at the regions of 298 K, we can see that the temperature resolution is less than ± 1 K. But the temperature variation in the 15-m section cannot be achieved correctly because the spatial region of temperature variation is shorter than the spatial resolution. The maximum temperature error of about 11 K is produced when the temperature is set at 331 K.

After applying the ASFDA, the restored temperature distribution is shown in Fig. 5. The boundary of the frequency intervals is set at 5 MHz. The values of λ are 1 ($<$5 MHz) and 10^8 ($\geq$5 MHz), respectively. It can be seen that the 15-m temperature variation information is achieved correctly. The restored temperatures of the five abnormal sections are 309.3, 316, 321.4, 326.8, and 332.9 K, respectively. In the range of 30-K temperature increment, the temperature accuracy is superior to ± 2 K. The results demonstrate that a spatial resolution of 15 m is realized with the pulse width of 300 ns. Although the temperature resolution at the regions of 298 K is lower than that of conventional method from the experimental results, the deconvolution algorithm can be used as a beneficial complement for the FRDTS using conventional method to realize accurate locating and temperature monitoring for the sharp temperature variations.

The dispersion-induced input light broadening and the walk-off induced by the group velocity dispersion of backscattered light will affect the measurement result restored by the deconvolution algorithm. Generally, the linewidth of input light is not very wide. However, the linewidth of anti-Stokes backscattered light is usually about 20 nm limited by the BPF, which is much greater than the dispersion-induced input light broadening. Therefore, the walk-off of anti-Stokes backscattered light at different frequencies determines the minimum achievable spatial resolution improved by deconvolution algorithm. The dispersion-induced time delay of anti-

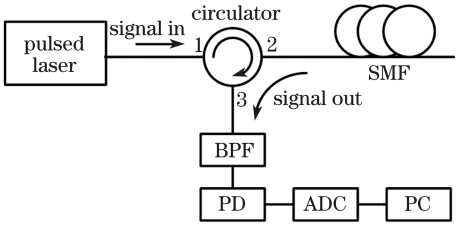

Fig. 3. Schematic diagram of the FRDTS. PD: photo detector; PC: personal computer.

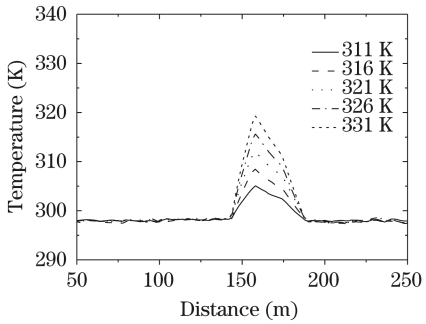

Fig. 4. Temperature distribution restored by traditional method.

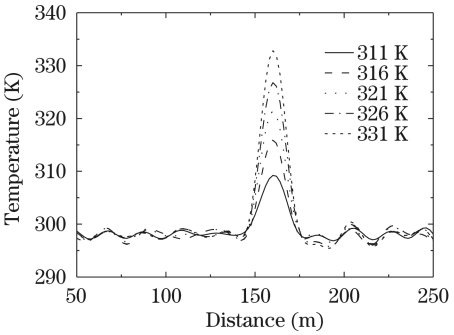

Fig. 5. Temperature distribution restored by ASFDA.

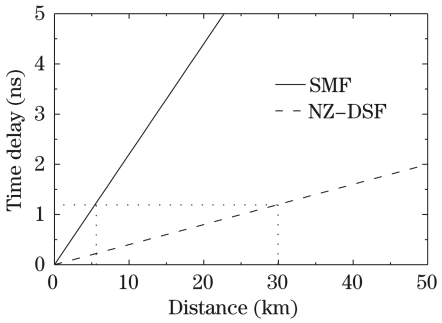

Fig. 6. Dispersion-induced time delay of anti-Stokes backscattered light at different frequencies with sensing distance for SMF and NZ-DSF.

Stokes backscattered light at different frequencies for SMF is calculated and shown in Fig. 6 with solid line, where the dispersion parameter is 11 ps/(nm·km) at the center wavelength of 1.45 μm. We define that the measurement result restored by the deconvolution algorithm can be acceptable if the time delay is smaller than 1% of the input light pulse width. According to the previous numerical simulation results, the spatial resolution can be enhanced by four times using the deconvolution algorithm. So if the minimum spatial resolution is 3 m, the input pulse width should be smaller than 120 ns. Then the time delay should be limited within 1.2 ns. As shown in Fig. 6, the maximum sensing distance for SMF is about 5.6 km. In order to increase the sensing distance, low dispersion fiber such as the non-zero dispersion shifted fiber (NZ-DSF) should be used. The dispersion parameter of NZ-DSF is typically 2 ps/(nm·km) at the center wavelength of 1.45 μm. As shown in Fig. 6 with dashed line, the maximum sensing distance for NZ-DSF can be extended to 30 km for the minimum spatial resolution of 3 m. If the minimum spatial resolution of 1 or 2 m is required, the maximum sensing distances are 10 and 20 km, respectively. These achieved spatial resolutions are almost the same as those of the top FRDTS products. That is to say, the deconvolution algorithm can be used to improve the spatial resolution in long distance FRDTS.

In conclusion, through theoretical analysis and experimental verification, it is demonstrated that the deconvolution algorithm can be applied in the data processing of FRDTS to improve the spatial resolution without reducing the pulse width of the light source. Numerical simulation shows that the spatial resolution is enhanced by four times using the frequency-domain deconvolution algorithm with high temperature accuracy and a little cost on the temperature resolution. In experiment, a spatial resolution of 15 m is realized using a MOPA light source with 300-ns pulse width, and at the same time the abnormal temperature can be restored well. We believe that the deconvolution algorithm can be used as a beneficial complement for the FRDTS to realize accurate locating and temperature monitoring for the sharp temperature variations. The dispersion-induced limitation of the minimum spatial resolution achieved by deconvolution algorithm is discussed. The results indicate that NZ-DSF is more suitable for long haul temperature sensing with the deconvolution algorithm.

References

1. D. Chen, W. Liu, Y. Zhang, J. Liu, R. Kan, M. Wang, X. Fang, and Y. Cui, Chin. Opt. Lett. **5,** 121 (2007).
2. K. Xie, Y. Rao, and Z. Ran, Acta Opt. Sin. (in Chinese) **28,** 569 (2008).
3. A. Sun, J. Chen, G. Li, L. Wang, L. Chang, and Z. Lin, Chinese J. Lasers (in Chinese) **34,** 503 (2007).
4. L. Zhang, Y. Liao, Z. Ou, Y. Liu, Z. Dai, Z. Peng, and D. Wang, Acta Opt. Sin. (in Chinese) **27,** 400 (2007).
5. H. Liu, S. Zhuang, Z. Zhang, and C. Feng, Proc. SPIE **5634,** 225 (2005).
6. A. H. Hartog, J. Lightwave Technol. **1,** 498 (1983).
7. X. Feng, L. Zhang, and X. Liu, Chin. Opt. Lett. **5,** 99 (2007).
8. R. Bernini, A. Minardo, and L. Zeni, IEEE Photon. Technol. Lett. **16,** 1143 (2004).
9. S. Fu, C. Wu, Y. Li, and X. Dong, Proc. SPIE **5634,** 241 (2005).
10. A. Bennia and S. M. Riad, IEEE Trans. Instrum. Meas. **39,** 358 (1990).
11. M. A. Farahani and T. Gogolla, J. Lightwave Technol. **17,** 1379 (1999).
12. G. Yilmaz and S. E. Karlik, Sens. Actuat. A **125,** 148 (2006).